Chemical Physics Impact 6 (2023) 100226

Contents lists available at ScienceDirect

Chemical Physics Impact

journal homepage: www.sciencedirect.com/journal/chemical-physics-impact

Spectroscopic characterization, electronic transitions and pharmacodynamic analysis of 1-Phenyl-1,3-butanedione: An effective agent for antipsychotic activity

M. Lawrence [a,b], E. Isac Paulraj [a,*], P. Rajesh [b]

[a] Department of Physics, Loyola Institute of Technology, Palanchur, Chennai, Tamil Nadu 600123, India
[b] Department of Physics, Vels Institute of Science, Technology and Advanced Studies (VISTAS), Chennai, Tamil Nadu 600117, India

ARTICLE INFO

Keywords:
DFT
FT-IR
FT-Raman
UV-Vis
Molecular docking

ABSTRACT

The density functional theory with the Becke, 3-parameter, Lee–Yang–Parr (B3LYP) technique and the 6-311++G(d,p) basis set is used to optimize the compound 1-Phenyl- 1,3-butanedione (1P1 3B). The 1-phenyl-1,3-butanedione may be obtained in good yield by first preparing a triketone from acetylacetone and a halogenated benzoyl derivative in the presence of a metal halide and tertiary amine in an organic solvent, and then deacetylating the triketone in the presence of an acid. The geometric characteristics of the featured molecule are calculated, and the vibrational frequencies with potential energy distribution (PED) are determined and compared to experimental data. The time-dependent density-functional theory (TD-DFT) technique was used to compute the frontier Molecular Orbitals. Using the HOMO-LUMO energy values, further electronic properties for 1P1 3B were determined. The reactive sites were estimated using the Electron Localisation Function (ELF), and the Molecular Electrostatic Potential (MEP). As a direct consequence of this, the whole molecule's electrophilic and nucleophilic areas have been mapped out. Natural bond orbital (NBO) calculations were used to investigate the delocalization of electron density. The drug likeness features of 1P13B were investigated. The Ramachandran plot is used to study the stability of hydrolase and antibody proteins. The headline molecule is subjected to molecular docking research in order to better understand its biological activities, as well as the minimal binding energy and hydrogen bond interactions.

1. Introduction

Because of the expanding use of a large variety of heterocyclic compounds, such as insecticides, herbicides, medicines, and so on, progress in heterocyclic chemistry has been quite rapid in recent decades [1–4]. Intensive research into synthetic chemicals that are often analogues of recognized pharmacological substances results in the creation of novel medications. For the purpose of researching keto-enol equilibria in aqueous acid and micellar solutions, 1-Phenyl-1,3-butanedione (1P1 3B) has been utilized as a model for the 1,3-dicarbonyl molecule [5]. Quantum chemistry and gas-phase electron diffraction are two more methods that have been utilized in its investigation. It is utilized in the pharmaceutical industry as an intermediary. 1P1 3B is a white color crystal with a melting point of 61°C and boiling point of 261-262°C. It is soluble in water, benzene, chloroform, carbon tetrachloride, alcohol, ether and concentrated alkali solution. It gives a long-lasting pungent smell. This is a balsamic fragrance and flavoring agent with a vanilla-woody scent. It is added to dishes that need a balsamic, amber, heather, oriental, or vanilla flavor. It easily absorbs moisture.

The compound is important both biologically and chemically [6–9]. The stability of heterocyclic compounds is determined by the ring size. Rings with three or four members are moderately unstable, but rings with five or six members are quite stable [10–13]. The chemical compound known as 1-phenyl-1,3-butanedione (1P1 3B) has the formula $C_{10}H_{10}O_2$ and a molecular mass of 162.19 g/mole. An examination of the relevant literature indicates that a significant number of studies have been conducted to get benzoylacetone derivatives. As the 1P13B has not been documented in the literature, we employ spectroscopy and quantum chemical simulations to characterize and explain its features. The objective of this study is to offer a comprehensive explanation of the 1P1 3B molecule based on both theoretical and empirically observed values.

* Corresponding author.
E-mail address: isacpaulraj@gmail.com (E.I. Paulraj).

https://doi.org/10.1016/j.chphi.2023.100226
Received 30 March 2023; Received in revised form 1 May 2023; Accepted 11 May 2023
Available online 13 May 2023

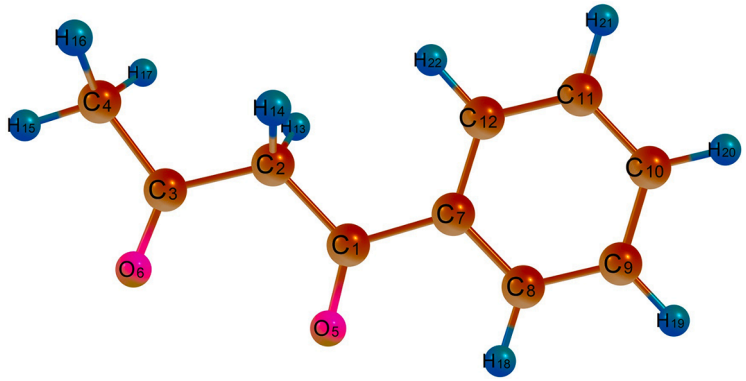

Fig. 1. Representation of the atoms in the 1P1 3B molecule's optimal structure.

In this paper, both the theoretical and experimental spectroscopic characterizations of 1P1 3B are presented. It is possible to determine geometry of molecule, frequency of vibration, surface analysis of the molecule, and chemical reactivities of the molecule by using density functional theory in conjunction with the B3LYP technique and the 6-311++G(d,p) basis set [14–19]. Potential Energy Scan analysis was used to investigate molecule stability (PES). Using their essential chemical characteristics, UV-Vis and HOMO-LUMO studies are utilized to determine the electronic properties. Molecular reactivities are calculated using the MEP surface studies. In addition, molecular docking, which is also known as protein-ligand analysis, has been used to explain the biological activity of antipsychotic nature in relation to bipolar disorders for 1P13B [20–23]. The purpose of this work is to provide an overview of the applications of spectroscopic methods for the structural analysis, electronic transitions, and quantum chemical characterization of 1-phenyl-1,3-butanedione. The interpretation of FTIR, FT-Raman, and UV-Vis spectroscopic data using density functional theory is the most essential of the several approaches. The utility of these approaches lies in their ability to determine and validate molecular structures, and the molecular docking provides information regarding the biological activity of the molecule [24–27].

2. Experimental details

1P1 3B with a purity of 99% was purchased from Sigma Aldrich. The study was completed without further purifications. The FT-Raman spectrum with a resolution of 2cm^{-1} was obtained using a Nd-YAG laser with a wavelength of 1064 nm and a power of 100 mW in the range 4000-100 cm^{-1} equipped in a BRUKER RFS 27 at IIT SAIF in Chennai, India. The FT-IR spectrum of 1P1 3B was reported with a resolution of 1.0 cm^{-1} in the region 4000-400 cm^{-1}.The data was obtained using a PERKINELMER FT-IR spectrophotometer at SAIF IIT Chennai, India, which employs the KBr pellet technique. The UV-VIS analysis on 1P13B was performed in the wavelength range 200-800 nm with dimethyl sulfoxide (DMSO) as the solvent.

3. Computational details

DFT (B3LYP) with 6-311G++(d,p) as the theory level was used to calculate the quantum chemical properties of 1P1 3B [28,29]. This particular basis set differs from others in that it provides a more in-depth explanation and splits the orbitals that are used for valence and core electrons. To improve the approximations, the basis set was polarized with (d, p) and diffused with (++). Chosen base set is enough for computing the final energy to an exact level. According to the research that has been done, the 6-311G++ (d, p) algorithm is highly efficient in terms of delivering appropriate computed geometries and energies at a reasonably low level of computing expense. GAUSSIAN 09W was used to optimize the structure. Using CHEMCRAFT [30], bond lengths and bond angles were computed for the molecule. Using the Gauss View 5.0 program, we were able to successfully complete the geometrical components [31]. The harmonic vibrational frequencies for this optimized structure were assigned using VEDA software [32]. In addition, WinX PRO [33] was used to generate the molecular electrostatic potential (MEP) map of the 1P1 3B molecule from the potential cube file generated by the Gaussian 09W application. To compare the experimental and theoretical vibrational wavenumbers, a scaling factor of 0.967 was used [34,35]. The results for UV were obtained using the TD-DFT/B3LYP theory. An estimate of the HOMO and LUMO energy levels was developed via the use of an analysis of the Frontier Molecular Orbital [36–38]. Calculations were also done on the electron density delocalization that occurred inside the molecule's donor and acceptor NBOs. This contributed to the evaluation of hyperconjugation and intramolecular interactions. For the purpose of producing Electron Localization Function (ELF) maps, MULTIWFN was used [39]. The DOS and PDOS spectra were generated using GAUSSSUM 2.2 [40]. AutoDock 4.2.6 [41] was used for molecular docking simulations. The protein-ligand interaction was investigated with the use of software applications including PyMOL [42], Discovery Studio [43], Ligplot [44] and Chimera [45].

4. Results and discussions

In the realms of biomaterials and computing, machine learning has recently become more popular. Using machine learning will be a time-saving and convenient option [46–49]. When compared to the experimental technique, the computational method saves money by reducing or eliminating chemical waste and development time for materials. DFT approaches primary advantage is an enormous improvement in computing accuracy with no corresponding increase in processing time. That's why this study employs a machine-learning based theory at the DFT level.

4.1. Geometry analysis

The geometrical properties of the 1P1 3B molecule, such as bond lengths and bond angles, were determined with the help of the DFT (B3LYP level of theory) technique [28,29] employing basis sets (6-311G++(d,p)), and the optimized scaled ball and stick model can be shown in Fig. 1. Maximum force (0.000406 a.u.) and displacement (0.000232 a.u.) converged for the 1P1 3B molecule, while the RMS gradient value for the potential energy surface converged to 0.000074 a. u. The dipole moment value was also determined to be 5.9767 Debye. Since, according to the literature review, the 1P1 3B crystal structure has not yet been published, the calculated structural parameters of the 1P1 3B molecule were connected via experimental XRD data [50] associated to the structure. The resulting parameter values are shown in Table 1. There is a little discrepancy between the experimental and calculated values for the 1P1 3B molecule because the computed values are

Table 1
Comparison of selected bond lengths and bond angles of the 1P1 3B molecule with XRD data.

Bond Length (Å)	Calculated	Exp[a]	Bond Angle (°)	Calculated	Exp[a]
C(1)-C(2)	1.523	1.402	C(2)-C(1)-O(5)	123.2	122.0
C(1)-O(5)	1.184	1.293	C(2)-C(1)-C(7)	116.7	122.7
C(1)-C(7)	1.511	1.481	C(1)-C(2)-C(3)	119.9	119.8
C(2)-C(3)	1.527	1.408	C(1)-C(2)-H (13)	108.3	121.3
C(2)-H(13)	1.088	1.076	C(1)-C(2)-H (14)	108.3	121.1
C(2)-H(14)	1.088	1.075	O(5)-C(1)-C(7)	120.0	116.2
C(3)-C(4)	1.518	1.495	C(1)-C(7)-C(8)	117.5	121.7
C(3)-O(6)	1.181	1.281	C(1)-C(7)-C (12)	123.6	118.9
C(4)-H(15)	1.081	1.060	C(3)-C(2)-H (13)	107.2	118.8
C(4)-H(16)	1.087	1.064	C(3)-C(2)-H (14)	107.2	118.6
C(4)-H(17)	1.087	1.050	C(2)-C(3)-C(4)	113.5	120.7
C(7)-C(8)	1.393	1.402	C(2)-C(3)-O(6)	125.1	117.3
C(7)-C(12)	1.390	1.405	H(13)-C(2)-H (14)	105.0	106.2
C(8)-C(9)	1.382	1.391	C(4)-C(3)-O(6)	121.4	117.3
C(8)-H(18)	1.073	1.079	C(3)-C(4)-H (15)	109.4	113.0
C(9)-C(10)	1.387	1.395	C(3)-C(4)-H (16)	110.4	110.7
C(9)-H(19)	1.075	1.087	C(3)-C(4)-H (17)	110.4	109.8
C(10)-C(11)	1.383	1.395	H(15)-C(4)-H (16)	109.5	108.4
C(10)-H(20)	1.076	1.086	H(15)-C(4)-H (17)	109.5	107.5
C(11)-C(12)	1.386	1.392	H(16)-C(4)-H (17)	107.5	107.2
C(11)-H(21)	1.075	1.092	C(8)-C(7)-C (12)	118.9	119.4
C(12)-H(22)	1.074	1.081	C(7)-C(8)-C(9)	120.6	120.0
C(7)-C(8)-H(18)	118.8	120.6			
C(7)-C(12)-C (11)	120.6	120.1			
C(7)-C(12)-H (22)	121.0	119.2			
C(9)-C(8)-H(18)	120.7	119.3			
C(8)-C(9)-C(10)	120.0	120.5			
C(8)-C(9)-H(19)	119.9	119.3			
C(10)-C(9)-H (19)	120.1	120.2			
C(9)-C(10)-C (11)	119.9	119.7			
C(9)-C(10)-H (20)	120.1	120.7			
C(11)-C(10)-H (20)	120.0	119.6			
C(10)-C(11)-C (12)	120.0	120.3			
C(10)-C(11)-H (21)	120.2	120.2			
C(12)-C(11)-H (21)	119.8	119.5			
C(11)-C(12)-H (22)	118.4	120.7			

[a] Experimental values taken from [50].

analyzed in gas phase and the experimental values are analyzed in solid phase. A total of ten C-H bonds, ten C-C bonds, and two C-O bonds make up the 1P1 3B. C-C bond lengths in 1P1 3B range from 1.382 to 1.527 Å. The bond length of the 1P1 3B aromatic hydrocarbons between 1.088 and 1.074. The bond with the longest length in 1P1 3B is C(2)–C(3) at 1.527Å with the experimental value of 1.408 Å.

4.2. Vibrational spectral analysis

Due to its 22 atoms, 1P1 3B will exhibit 60 different vibrational modes. Table 2 lists the molecule's wavenumbers (both theoretical and experimental), along with the accompanying vibrational assignments and intensities. Figs. 2 and 3 show the theoretical (scaled) and experimental vibrational spectra of 1P1 3B. The linear correlation (R^2) of the infrared spectroscopy data is analysed to assess the concordance between the FTIR and FT-Raman spectral responses. Experiment and theory both provide FTIR spectra with an R^2 of 0.99881. The R^2 value for comparing FT-Raman experiments and calculations is 0.99876. Quantitatively comparing IR spectra from experiment and theory has the potential to be a cutting-edge new way for evaluating quantum-chemical procedures.

4.2.1. C-H vibrations

At higher wavenumbers, asymmetric C–H bond stretching in 1P1 3B was observed. Typically, C–H stretching vibrations occur around 3000 cm^{-1} [51]. C–H bond stretching corresponds to the theoretical wavenumbers 3262 cm^{-1}, 3250 cm^{-1}, 3237 cm^{-1}, 3225 cm^{-1}, 3213 cm^{-1}, 3175 cm^{-1}. The C–H stretching may be seen as a peak in the FT IR spectrum at 3389 cm^{-1} and 3056 cm^{-1}, respectively. Vibrations may be detected for the methyl group in the ranges of 3000cm^{-1} and 2926 cm^{-1} or 2941cm^{-1} and 2905 cm^{-1} [52–55]. Peaks observed at 3073 cm^{-1}, 2924 cm^{-1} in the experimental FT-Raman spectrum correspond to the stretching of the methyl group. In the targeted region, the theoretical wavenumbers 3100cm^{-1}, 3074cm^{-1}, and 3062 cm^{-1} are seen. These theoretical observations were discovered to be consistent with experimental facts. Usually, the frequency shift may occur due to the interaction of intramolecular hydrogen with C=O and C-H vibrational modes [56,57]. Here the intramolecular hydrogen bond unaffected the C-H vibrations of 1P1 3B. The theoretical bending vibrations of the methyl group have wavenumbers of 1540cm^{-1}, 1491cm^{-1} and 1409 cm^{-1}. According to the literature, bending modes involving CH3 vibrations were observed in the area 1485-1400 cm^{-1} [58]. On the FT-IR spectra, experimental peaks for the same were identified at 1452 cm^{-1}. CH3 bending is represented by peaks at wavenumbers 1437 cm^{-1} in the FT Raman spectra.

4.2.2. C-C vibrations

The carbon–carbon stretching vibration occurs within the range of 1650–1100cm^{-1} [59]. On the FT-IR spectra at 1694 cm^{-1}, 1610 cm^{-1}, 1494 cm^{-1}, 1388 cm^{-1}, 1364 cm^{-1}, 1272 cm^{-1}, 1198 cm^{-1}, 1065 cm^{-1}, 1044 cm^{-1} and 1025 cm^{-1} and the FT-Raman spectrum at 1497 cm^{-1}, 1366 cm^{-1}, 1180 cm^{-1} and 1018 cm^{-1}, the same vibrations were observed. Theoretical C–C stretching vibrations have been detected between 1703 cm^{-1} and 1019 cm^{-1}. It reveals that theoretical predictions and actual observations correlate closely with one another as well as with the PED contributions of 60, 30, 76, 84, 12, 23, 11, 45, 31, 18 % respectively.

4.2.3. C=O vibrations

H-bonded C=O groups of 1-phenyl-1,3-butanedione is considerably located near the oxygen atom attached to the carbon atom linking to a phenyl group. The stretching vibration of the carbonyl group is observed in the range of 1850–1550 cm^{-1} [60,61]. The molecule exhibits a significant absorption peak at 1903 cm^{-1} and 1947 cm^{-1} in FT-IR and Raman spectra, respectively. Theoretically, the intramolecularly of H-bonded C=O groups are located at 1960 cm^{-1} and 1902 cm^{-1} with 86% and 88% of PED respectively [62,63].

4.3. Molecular electrostatic potential

By using color grading, the preferred site of the electrophile and nucleophile is clarified in terms of the molecule electrostatic potential. The dynamic binding location and reactive positions of the title chemical with the color regions are analysed using MEP [64,65]. Fig.4 displays the MEP diagram for the 1P1 3B. The oxygen atoms, which have a red hue and a negative potential, operate at the nucleophilic reactive

Table 2
Experimental and computed spectroscopic data and their vibrational assignments for 1P1 3B molecule.

Wavenumber(cm^{-1})				IR intensity		Raman activity		Vibrational assignments(%PED)
Experimental IR	Raman	Theoretical Unscaled	Scaled*	Absolute	Relative †	Absolute	Relative †	
3389(w)		3373	3262	4	1	89	58	ν CH(93)
		3360	3250	12	3	129	84	ν CH(89)
3056(w)		3347	3237	27	7	104	68	ν CH(88)
		3335	3225	11	3	98	64	ν CH(96)
		3322	3213	1	1	47	31	ν CH(89)
	3254(w)	3283	3175	17	4	92	60	ν CH(92)
		3226	3120	24	6	63	41	ν CH(92)
		3205	3100	2	1	11	8	ν CH(85)
3073(s)	3073(s)	3178	3074	9	3	154	100	ν CH(87)
2904(m)	2924(s)	3166	3062	4	1	50	33	ν CH(88)
		2026	1960	442	100	37	25	ν OC(86)
1903(w)		1966	1902	24	6	17	12	ν OC(88)
1733(s)		1785	1727	15	4	77	50	ν CC(63) + δ HCC(27)
1694(s)		1761	1703	6	2	9	6	ν CC(60) + δ HCC(10) + δ HCC(16)
1610(s)		1648	1594	1	1	1	1	δ HCC(61) + ν CC(30)
	1596(s)	1597	1545	12	3	8	6	δ HCH(78)
		1592	1540	24	6	2	2	ν CC(16) + δ HCC(38) + ν CC(18)
	1565(m)	1585	1533	12	3	9	6	δ HCH(81)
	1562(m)	1557	1506	17	4	4	3	τ HCCO(90)
		1541	1491	199	46	2	2	δ HCC(43) + ν CC(17)
1494(w)	1497(s)	1515	1466	12	3	1	1	γ CHHH(76)
1452(s)	1437(m)	1457	1409	1	1	2	2	δ HCC(80)
1388(w)	1366(m)	1355	1311	1	1	5	4	δ HCC(84)
1364(s)		1336	1292	18	5	3	2	δ HCC(60) + ν CC(12)
		1320	1277	41	10	26	17	ν CC(38) + δ HCC(13)
1272(s)		1290	1248	14	4	4	3	ν CC(23) + δ HCC(62)
	1266(s)	1260	1219	125	29	4	3	δ HCC(11) + δ HCC(23) + ν CH(16)
	1240(m)	1214	1174	7	2	7	5	ν CC(21) + δ HCC(10) + ν CC(26) + δ HCC(20) + ν CC(10)
1198(s)	1180(m)	1172	1134	1	1	1	1	δ HCC(11) + δ HCC(11) + τ HCCC(60)
	1154(m)	1149	1112	3	1	3	2	δ HCH(10) + τ HCCC(56)
		1123	1086	1	1	1	1	τ HCCC(91)
		1120	1084	1	1	12	8	δ HCC(21) + ν CC(62)
		1109	1073	1	1	1	1	τ HCCC(94)
		1085	1050	18	5	20	13	δ HCC(76)
1065(s)		1076	1041	35	8	34	23	ν CC(12) + ν CC(45)
1044(w)		1055	1021	2	1	1	1	τ HCCC(91)
1025(s)	1018(m)	1053	1019	22	5	13	9	δ HCC(12) + δ HCC(42) + ν CC(18)
974(s)	1004(s)	952	921	1	1	2	2	τ HCCC(82)
	972(m)	947	916	1	1	1	1	τ HCCC(73)
		912	882	2	1	11	8	δ HCC(15) + ν CC(42) + δ CCC(15)
839(s)		855	827	14	4	2	2	ν CC(21) + ν CC(39)
811(w)	802(m)	834	807	67	16	1	1	τ HCCC(86)
757(s)	770(s)	757	733	38	9	1	1	τ HCCC(93)
	768(w)	728	704	6	2	10	7	δ HCC(57) + ν CC(12)
690(s)	674(s)	673	651	1	1	7	5	δ HCC(87)
		651	630	8	2	1	1	τ HCCO(77)
573(m)		584	565	63	15	4	3	δ HCC(10) + δ CCO(54)
514(s)		504	488	5	2	1	1	τ HCCC(79)
	474(w)	495	479	1	1	2	2	δ HCC(17) + δ HCC(11) δ HCC(18) + ν CC(25)
		450	436	1	1	1	1	τ HCCC(96)
402(m)		428	414	1	1	1	1	τ HCCO(94) + τ HCCO(19)
	382(w)	378	366	10	3	2	2	δ CCC(65)
	294(s)	306	296	1	1	4	3	ν CC(13) + δ CCC(52)
	219(s)	244	236	1	1	2	2	δ CCC(59)
	189(w)	161	156	1	1	3	2	τ HCCO(65)
		120	117	3	1	1	1	δ CCC(89)
	95(s)	99	96	1	1	1	1	τ HCCO(76) + τ HCCO(10)
	74(s)	49	48	10	3	1	1	τ HCCO(79) + τ HCCO(11)
		24	24	1	1	2	2	τ HCCO(16) + τ HCCO(37) + τ HCCC(17)
		17	17	1	1	1	1	τ HCCO(10) + τ HCCC(70)

ν-stretching, δ-in-plane bending, γ- out-of-plane bending and τ-torsion. s-strong, m-medium, w-weak.
* scaling factor 0.967 for B3LYP/6-311++G(d,p) basis set.
† Normalised to 100.

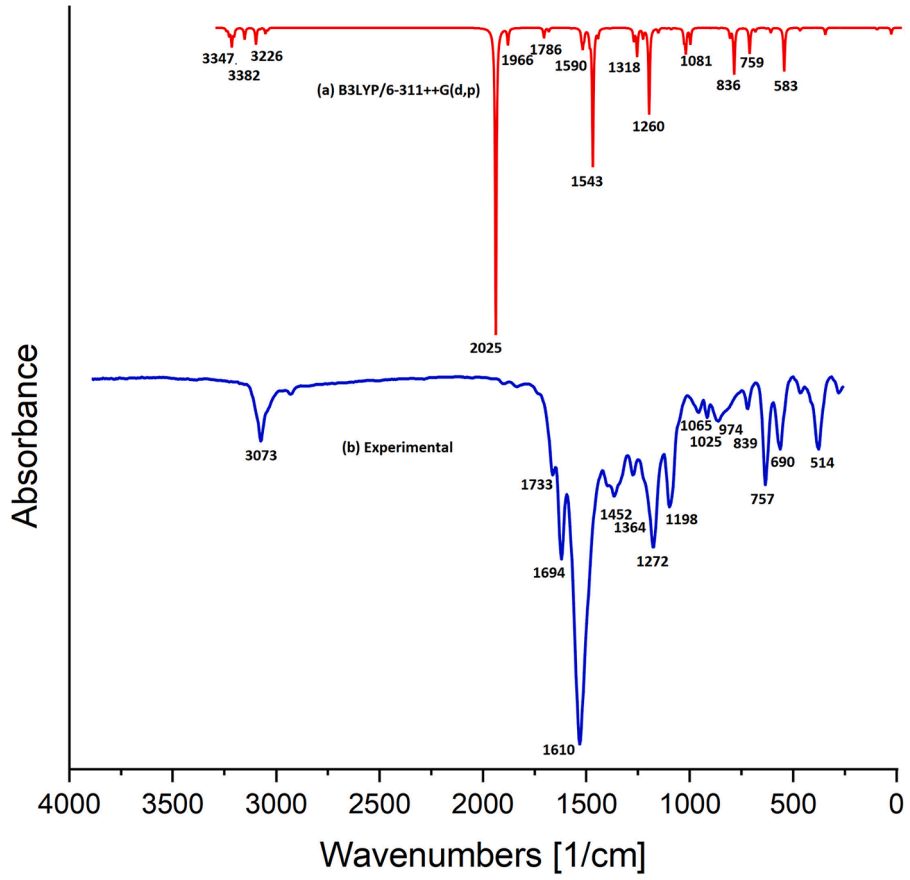

Fig. 2. The FT-IR spectra of the 1P1 3B molecule, both calculated and experimentally obtained.

site. The positive charge, which is concentrated on H17 and H13 and can serve as an electrophilic reactive site, is denoted by the color blue. The area between the color codes for –0.123 e^0 and +0.123 e^0 on the MEP diagram of the compound under examination. The active sites of the headline compound have been revealed using MEP visualization, and these sites may now be taken into account for docking with various proteins.

4.4. Donor-acceptor interactions

The NBO method improves our understanding of intra and intermolecular interactions by providing proof of their occurrence in both occupied and virtual orbital regions. With the help of the fock matrix, the interaction is analysed. The B3LYP method with 6–311++G(d,p) basis set is used in the performance of the NBO analysis for 1P1 3B. Donor-acceptor pairings and values of stabilisation energy are figured out [66] and displayed in Table 3. The coincidental orbital passage that takes place between the σ(C–C) and σ*(C–C) orbitals of bonds ultimately results in intramolecular charge transfer (ICT) and the stabilization of the system [67,68]. Due to conjugative interactions, electrons from carbon atoms σ(C1–C7) disperse to the antibonding carbon atoms σ*(C2–Cl3), σ*(C7–C8), σ* (C7–C12),σ* (C8–C9),σ* and (C11–C12) with stabilization energies of 1.64, 1.67, 2.12, 2.48, and 2.18 kcal/mol respectively. Anti-bonding electron of π*(C1–O5), π*(C8– C9), and π*(C10–O11) derived from the bonding electron on π (C7–C12) with moderate stabilization energy 16.28, 19.84 and 19.00 kcal/mol respectively. The NBO analysis anticipated a strong σ* interaction due to the lone pairs of oxygen atoms LP(2)O6 (C2-C3) with the stabilizing energy of 26.94 kcal/mol. The delocalization of the electron from π (C8–C9) distributes anti-bonding π* (C7–C12) and π* (C10–C11) with stabilizing energies of 19.84 and 21.91 kcal/mol, respectively. It was found that there was a robust interaction as a consequence of the delocalization of the π(C10–C11) to the π*(C7–C12) state, which had a high stabilising energy of 21.77 kcal/mol.

4.5. Electron localisation function and localised orbital locator

The electron localisation function (ELF) and the localised orbital locator (LOL) are the methods that are used during the process of computing the amount of electron density that is present in the compounds. The study of covalent bonds is carried out by both of them, and they reveal the areas of the molecular space in which the probability of a verdict being reached on an electron pair is high [69,70]. Figs. 5 and 6 present the color-filled projection map, as well as the vector field of ELF and LOL with the contour map, all of which were derived from the Multiwfn software for the 1P1 3B molecule. These maps are supposed to fall within the range of 0 – 1.0, which indicates that the chemical components that they include are comparable. If the value of ELF is between 0.5 and 1.0 on the figure, then they contain both bonding and non- bonding localized electrons. On the other hand, they have delocalized electrons if the value is below 0.5. Even though the interpretations are quite similar to one another, LOL provides a more comprehensive and spotless description than ELF does. The upper end of the scale is represented by the color red, while the lower end of the scale is represented by the color blue in this scale. The regions surrounding C1, C2, C3, C4, C7, C8, C9, C10, C11, and C12 reveals strong localization of both bonding and nonbonding electrons. On the other hand, the regions around H16, H18, H19, H20, H21, and H22 suggest that the electrons are predicted to be delocalized due to their smaller values. In LOL, the covalent areas that have a high LOL value are represented by red zones that are displayed between carbon atoms and hydrogen atoms. These regions include C4-H16, C7-H16, C8-H18, C9-H19, C10-H20,

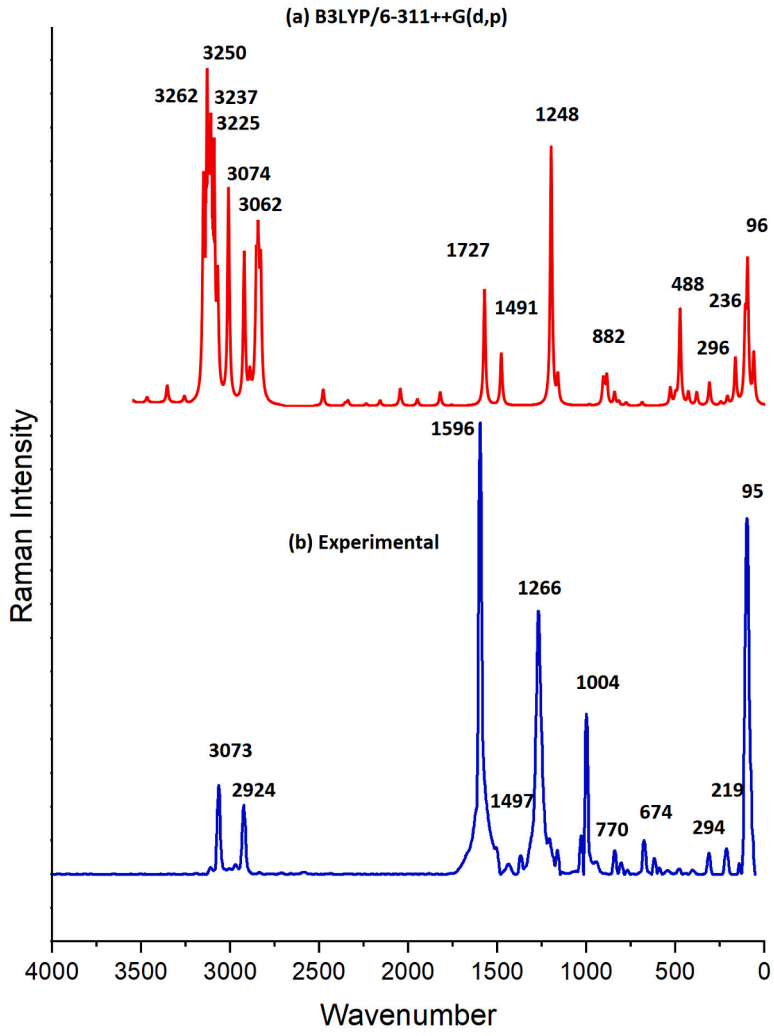

Fig. 3. The FT-Raman spectra of the 1P1 3B molecule, both calculated and experimentally obtained.

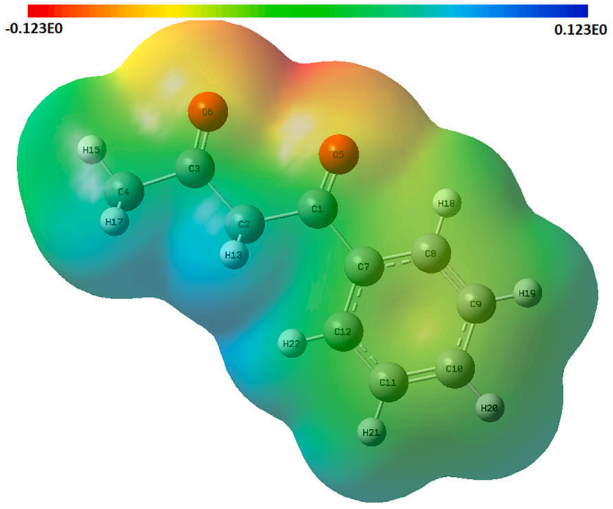

Fig. 4. Surface map of the 1P1 3B molecule's electrostatic potential.

C11-H21, and C12-H22.

4.6. *Electronic properties*

Both the experimental and theoretical UV-Vis spectra of 1B1 3P have been done in DMSO solution, with the latter being calculated using TD-DFT/6-311++G (d,p) as the basis set. Table 4 displays the important parameters during electronic transitions, including absorption wavelength (λ), excitation energy (E), and oscillator strengths (f) as estimated experimentally and theoretically (TD-DFT). Fig. 7 depicts theoretical and experimental absorption values at 335, 281, 262, 249 nm, which correspond to the 0.0016, 0.2257, 0.0307, 0.0167 oscillator frequencies, respectively. The major contributions come from the H-2 LUMO (13%), HOMO LUMO (83%), HOMO L+1 (34%), HOMO L+2 (43%), H-2 LUMO (75%), HOMO - LUMO (14%), H-3 LUMO (33%), H-1 LUMO (50%) Energy gap (E) values for 1B1 3P include 3.69 eV (H-2 LUMO; 13%), (HOMO - LUMO; 83%), and 3.39 eV, with an experimental value of 3.07 eV. As a result, the experimental peaks correspond well with the calculated UV-Vis spectrum. FMOs serve a key function in interactions of the molecules. Furthermore, the energy differential between molecular orbitals gives a substantial viewpoint on the optical, electrical, and chemical characteristics of the molecule under research. The HOMO is the electron donor that contributes to a filled state, whereas the LUMO is the electron acceptor that contributes to an empty state [71]. The HOMO and LUMO energies, as well as their orbital energy gaps, were calculated using the B3LYP/6-311++G(d,p) approach. Fig. 8 depicts simulated

Table 3
Second order perturbation theory analysis of Fock matrix in NBO basis of 1P1 3B molecule.

Donor	Type	ED/e (qi)	Acceptor	Type	ED/e (qi)	E(2)[a] Kcal/mol	E(j)-E(i)[b] a.u	F(I,j)[c] a.u
C1 - C2	σ	1.98521	C1 - O5	σ*	0.00878	1.05	1.3	0.033
			C3 - C4	σ*	0.06134	1.65	1.02	0.037
			C7 - C8	σ*	0.02193	1.9	1.22	0.043
C1 - O5	σ	1.99589	C1 - C7	σ*	0.07417	1.06	1.55	0.037
			C7 - C12	σ*	0.36789	1.12	1.72	0.039
C1 - O5	π	1.97501	C2 - H13	σ*	0.01036	1.39	0.81	0.03
			C2 - H14	σ*	0.01036	1.39	0.81	0.03
			C7 - C12	π*	0.36789	4.78	0.41	0.044
C1 - C7	σ	1.97909	C2 - C3	σ*	0.07412	1.64	1.03	0.037
			C7 - C8	σ*	0.02193	1.67	1.23	0.04
			C7 - C12	σ*	0.36789	2.12	1.23	0.046
			C8 - C9	σ*	0.01538	2.48	1.25	0.05
			C11 - C12	σ*	0.01656	2.18	1.23	0.046
C2 - C3	σ	1.98607	C1 - C7	σ*	0.07417	1.98	1.06	0.042
			C4 - H15	σ*	0.00489	1.07	1.11	0.031
C2 - H13	σ	1.95596	C1 - O5	σ*	0.00878	1.95	1.19	0.043
			C1 - O5	π*	0.11208	4.43	0.56	0.045
			C3 - O6	σ*	0.01275	2.12	1.19	0.045
			C3 - O6	π*	0.01275	4.55	0.56	0.045
C2 - H14	σ	1.95596	C1 - O5	σ*	0.00878	1.95	1.19	0.043
			C1 - O5	π*	0.11208	4.43	0.56	0.045
			C3 - O6	σ*	0.01275	2.12	1.19	0.045
			C3 - O6	π*	0.01275	4.55	0.56	0.045
C3 - C4	σ	1.99058	C1 - C2	σ*	0.06134	2.17	1.02	0.043
C3 - O6	π	1.98433	C2 - H13	σ*	0.01036	1.31	0.81	0.029
			C2 - H14	σ*	0.01036	1.31	0.81	0.029
			C4 - H16	σ*	0.00603	1.5	0.83	0.032
			C4 - H17	σ*	0.00603	1.5	0.83	0.032
C4 - H15	σ	1.98924	C2 - C3	σ*	0.07412	3.57	0.9	0.051
C4 - H16	σ	1.97624	C3 - O6	σ*	0.01275	1.77	1.19	0.041
			C3 - O6	π*	0.01275	4.46	0.55	0.045
C4 - H17	σ	1.97624	C3 - O6	σ*	0.01275	1.77	1.19	0.041
			C3 - O6	π*	0.01275	4.46	0.55	0.045
C7 - C8	σ	1.9736	C1 - C2	σ*	0.0687	1.94	1.08	0.041
			C1 - C7	σ*	0.07417	1.74	1.12	0.04
			C7 - C12	σ*	0.36789	4.06	1.28	0.064
			C8 - C9	σ*	0.01538	2.62	1.29	0.052
			C8 - H18	σ*	0.0162	1.32	1.2	0.036
			C9 - H19	σ*	0.01296	2.32	1.19	0.047
			C12 - H22	σ*	0.0139	2.58	1.18	0.049
C7 - C12	σ	1.97632	C1 - O5	σ*	0.00878	1.26	1.37	0.037
			C1 - C7	σ*	0.07417	1.57	1.13	0.038
			C7 - C8	σ*	0.02193	4.06	1.29	0.065
			C8 - H18	σ*	0.0162	2.03	1.22	0.044
			C11 - C12	σ*	0.01656	3	1.29	0.056
			C11 - H21	σ*	0.01264	2.15	1.2	0.045
			C12 - H22	σ*	0.0139	1.48	1.19	0.038
C7 - C12	π	1.65111	C1 - O5	π*	0.11208	16.28	0.29	0.065
			C8 - C9	π*	0.28746	19.84	0.29	0.069
			C10 - C11	π*	0.32016	19	0.29	0.067
C8 - C9	σ	1.97945	C1 - C7	σ*	0.07417	3.06	1.13	0.053
			C7 - C8	σ*	0.02193	3.1	1.29	0.056
			C8 - H18	σ*	0.0162	1.44	1.21	0.037
			C9 - C10	σ*	0.01705	2.69	1.29	0.053
			C9 - H19	σ*	0.01296	1.29	1.2	0.035
			C10 - H20	σ*	0.01266	2.38	1.19	0.048
C8 - C9	π	1.65093	C7 - C12	π*	0.36789	19.84	0.28	0.067
			C10 - C11	π*	0.32016	21.91	0.28	0.071
C8 - H18	σ	1.9797	C7 - C8	σ*	0.02193	1.23	1.1	0.033
			C7 - C12	σ*	0.36789	4.41	1.11	0.062
			C8 - C9	σ*	0.01538	1.01	1.12	0.03
			C9 - C10	σ*	0.01705	3.79	1.1	0.058
C9 - C10	σ	1.98054	C8 - C9	σ*	0.01538	2.71	1.3	0.053
			C8 - H18	σ*	0.0162	2.35	1.21	0.048
			C9 - H19	σ*	0.01296	1.26	1.2	0.035
			C10 - C11	σ*	0.01655	2.66	1.29	0.052
			C10 - H20	σ*	0.01266	1.25	1.19	0.034
			C11 - H21	σ*	0.01264	2.47	1.19	0.048
C9 - H19	σ	1.98224	C7 - C8	σ*	0.02193	3.9	1.11	0.059
			C8 - C9	σ*	0.01538	1.01	1.13	0.03
			C10 - C11	σ*	0.01655	3.66	1.12	0.057
C10 - C11	σ	1.98038	C9 - C10	σ*	0.01705	2.64	1.29	0.052
			C9 - H19	σ*	0.01296	2.35	1.2	0.047

(*continued on next page*)

Table 3 (*continued*)

Donor	Type	ED/e (qi)	Acceptor	Type	ED/e (qi)	E(2)[a] Kcal/mol	E(j)-E(i)[b] a.u	F(I,j)[c] a.u
			C10 - H20	σ*	0.01266	1.27	1.2	0.035
			C11 - C12	σ*	0.01656	2.77	1.29	0.053
			C11 - H21	σ*	0.01264	1.32	1.19	0.036
			C12 - H22	σ*	0.0139	2.35	1.19	0.047
C10 - C11	π	1.65308	C7 - C12	π*	0.36789	21.77	0.29	0.071
			C8 - C9	π*	0.28746	18.15	0.29	0.066
C10 – H20	σ	1.98249	C8 - C9	σ*	0.01538	3.62	1.13	0.057
			C11 - C12	σ*	0.01656	3.75	1.12	0.058
C11 - C12	σ	1.97888	C1 - C7	σ*	0.07417	3.57	1.13	0.057
			C7 - C12	σ*	0.36789	3.46	1.29	0.06
			C10 - C11	σ*	0.01655	2.72	1.29	0.053
			C10 - H20	σ*	0.01266	2.39	1.19	0.048
			C11 - H21	σ*	0.01264	1.26	1.19	0.035
			C12 - H22	σ*	0.0139	1.4	1.19	0.036
C11 - H21	σ	1.98236	C7 - C12	σ*	0.36789	3.93	1.12	0.059
			C9 - C10	σ*	0.01705	3.64	1.12	0.057
C12 - H22	σ	1.98099	C7 - C8	σ*	0.02193	4.04	1.12	0.06
			C7 - C12	σ*	0.36789	1.19	1.12	0.033
			C10 - C11	σ*	0.01655	3.66	1.13	0.057
O5	LP(1)	1.97755	C1 - C2	σ*	0.0687	1.41	1.05	0.035
			C1 - C7	σ*	0.07417	2.02	1.09	0.042
	LP(2)	1.87169	C1 - C2	σ*	0.0687	25.67	0.65	0.117
			C1 - C7	σ*	0.07417	23.16	0.68	0.114
O6	LP(1)	1.97658	C2 - C3	σ*	0.07412	1.74	1.04	0.039
			C3 - C4	σ*	0.06134	1.89	1.05	0.04
	LP(2)	1.87323	C2 - C3	σ*	0.07412	26.94	0.64	0.119
			C3 - C4	σ*	0.06134	23.85	0.64	0.112

[a] E2 represents stabilization energy.
[b] E(j)-E(i) represents the donor i and acceptor j energy difference.
[c] F(i,j) represents the Fock matrix element.

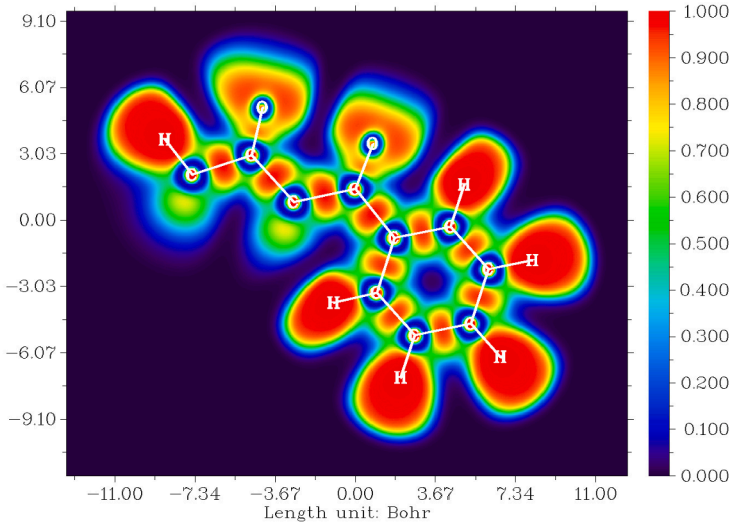

Fig. 5. Electron localisation function (ELF) of 1P1 3B.

FMOs with a positive phase in green and a negative phase in red to reflect charge transfer inside the molecule. The computed band gap energy value of 1P1 3B Energy gap 10.239 (eV) supports the molecule's chemical stability. In addition, the values of the HOMO and LUMO orbitals are associated with the ionization potential and electron affinity of the molecule. Electronic charge, electronegativity, chemical hardness, chemical softness (S), chemical potential (μ), and electrophilicity index (χ) were all predicted for 1P1 3B, and the results are reported in Table 5. The parameters specified by the relationship as,

$$\text{Chemical Potential } \mu = 1/2(\text{ELUMO} + \text{EHOMO}) \quad (1)$$

$$\text{Electro negativity} \chi = -1/2(\text{ELUMO} + \text{EHOMO}) \quad (2)$$

$$\text{Chemical hardness } \eta = 1/2(\text{ELUMO} - \text{EHOMO}) \quad (3)$$

$$\text{Electrophilicity index } \omega = \mu^2/2\eta \quad (4)$$

$$\text{Chemical Softness S} = 1/2\eta \quad (5)$$

Increasing chemical hardness and decreasing softness value indicate a stable compound. The compound was found to have a hardness of 5.1645 and a softness of 0.9681. The chemical has biological action because of its low electrophilicity index value of 1.8671.

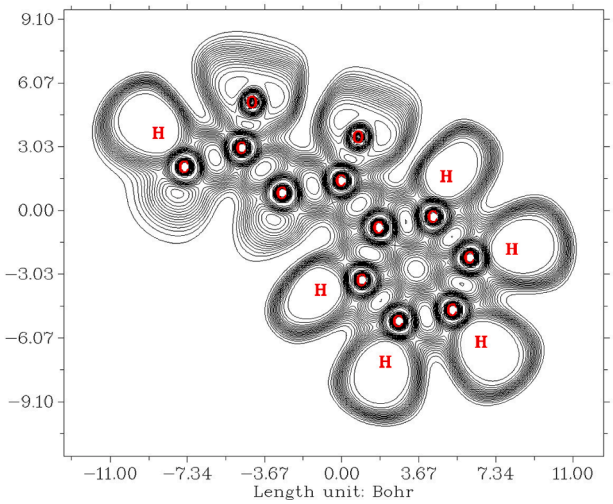

Fig. 6. Contour line map of the Electron Localisation Function (ELF) of 1P1 3B.

4.7. Density of energy states

Neighbouring orbitals in the border area may show the quasi-degenerate energy levels. In these circumstances, HOMO and LUMO alone might not be sufficient to provide a useful description of the boundary orbitals. As a result, the total and projected densities of states (TDOS and PDOS, respectively) were examined. The TDOS, PDOS and OPDOS are plotted in Figs. 9 and 10 respectively. In the DOS plot, the orbital HOMO is shown by the color green, and the orbital LUMO is shown by the color red. A binding interaction was used to verify the PDOS's positive value, an anti-bonding interaction was used to verify the PDOS's negative value, and a non-binding interaction was used to verify the PDOS's near-zero value [72]. In the boundary region, nearby orbitals may have energy levels that are almost the same. The projected density of state plot (PDOS) is primarily responsible for introducing the arrangement of the fragment orbitals that contribute to the molecular orbitals that are shown in Fig. 10.

4.8. Drug likeness

In Table 6, a summary of the drug similarity characteristics that were analysed can be seen. The number of hydrogen bond donors (HBD), the number of hydrogen bond acceptors (HBA), the number of rotatable bonds, the value of A logP, and the value of topological polar surface area (TPSA) are all included in these parameters. There is a correlation between the values of 1-phenylbutane-1,3-dione and the rule of five developed by Lipinski [73,74]. As a direct result of this, the value of HBD is 0 and the value of HBA is 2, and both of these values are less than the onset value of 10, which is 5, respectively. The molecule has one bond that may rotate freely. The value of A logP is 0.725, which is less than the cut-off number of 5, which is understood to be the bare minimum amount that may be considered acceptable. The TPSA of the chemical is much less than the value that is considered to be unsafe. According to the criteria shared by pharmaceutical drugs, the highlighted chemical has useful pharmacological properties.

4.9. Ramachandran plot

Examining the degree to which protein molecules are stable may be accomplished with the use of the Ramachandran plot. Moreover, it offers information that may be used for identifying, predicting, and confirming the structures of proteins. Protein dihedral angles are shown on a two-dimensional plane at several sites where stable conformations are known to exist along the protein's backbone [75,76]. The Ramachandran plots for the proteins 7EOA, 6XSU, and 5K59 are shown in Figs. 11-13. This demonstrates that the proportion of allowed regions in both proteins is more than ninety percent. In addition to that, the structures of these proteins include a substantial number of residues. In addition, none of the proteins has any residues in the places that are specifically prohibited from having them. In all, there were 259 residues in 7EOA, but 696 in 6XSU. The difference may be attributed to the number of residues present in each molecule. The number of residues of a protein called 5K59, which has the ability to neutralize antibodies, was 1982.

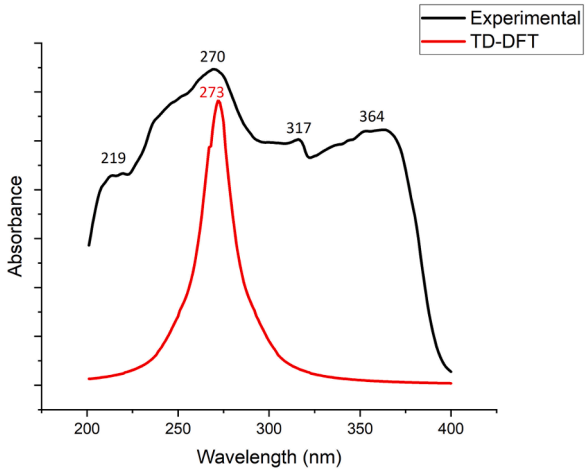

Fig. 7. Experimental and theoretical UV-Vis spectra of 1P13B in DMSO solution.

Table 4
The computed and experimental UV-Vis wavelengths of 1P1 3B using DMSO as solvent.

Computed No.	Wavelength (nm)	Band Gap (eV)	Energy (cm^{-1})	Oscillatory Strength	Assignments (Major contributions)	Experimental Wavelength max (nm)	Band Gap (eV)
1	335	3.69	29770.73	0.0016	H-2->LUMO (13%), HOMO->LUMO (83%)	364	3.07
2	281	4.41	35564.21	0.2257	HOMO->L+1 (34%), HOMO->L+2 (43%)	317	3.88
3	262	4.73	38152.44	0.0307	H-2->LUMO (75%), HOMO->LUMO (14%)	270	4.68
4	249	4.97	40094.63	0.0167	H-3->LUMO (33%), H-1->LUMO (50%)	219	5.72
5	231	5.35	43153.89	0.0201	HOMO->L+1 (57%), HOMO->L+2 (34%)		
6	227	5.46	44027.39	0.0057	H-3->LUMO (53%), H-1->LUMO (39%)		
7	214	5.78	46605.94	0.0002	H-2->L+1 (42%), H-2->L+2 (39%), HOMO->L+2 (18%)		
8	198	6.24	50305.61	0.0213	H-2->L+1 (44%), H-2->L+2 (51%)		
9	195	6.36	51100.87	0.0307	H-3->L+1 (17%), H-1->L+1 (49%), H-1->L+2 (24%)		
10	194	6.39	51541.25	0.0003	HOMO->L+3 (87%)		

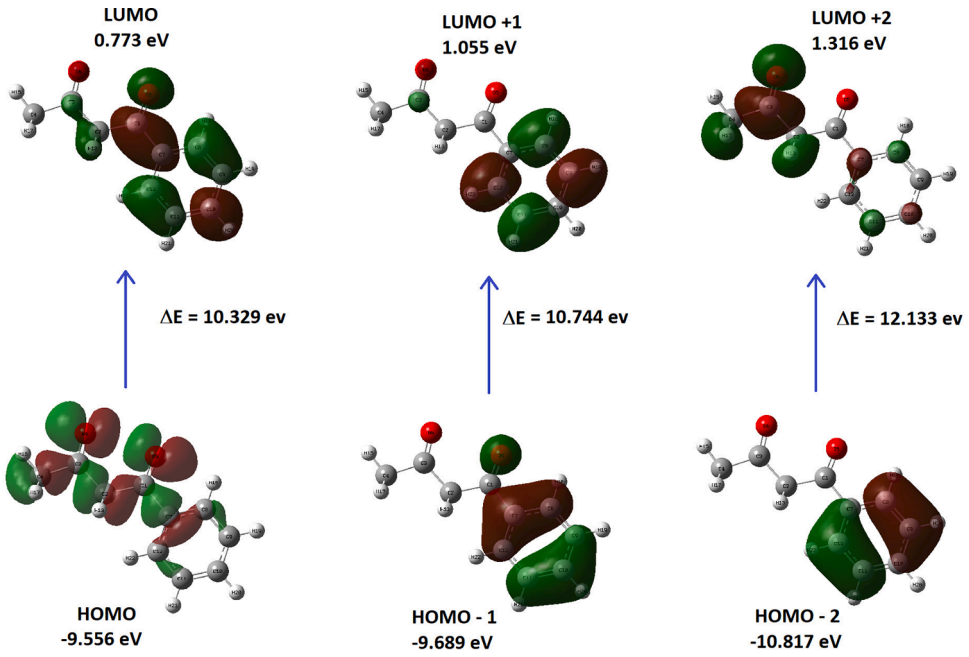

Fig. 8. Frontier molecular orbital diagram of 1P13B with band gap values.

Table 5
Second order perturbation theory analysis of Fock matrix in NBO basis of 1P1 3B molecule.

Parameters	Values (eV)
E_{HOMO} (eV)	-9.556
E_{LUMO} (eV)	0.773
Energy gap (eV)	10.329
Ionization potential (I)	9.556
Electron affinity (A)	-0.773
Electronegativity (χ)	4.3915
Chemical potential (μ)	-4.3915
Chemical Hardness (η)	5.1645
Chemical softness (S)	0.9681
Electrophilicity (ω)	1.8671

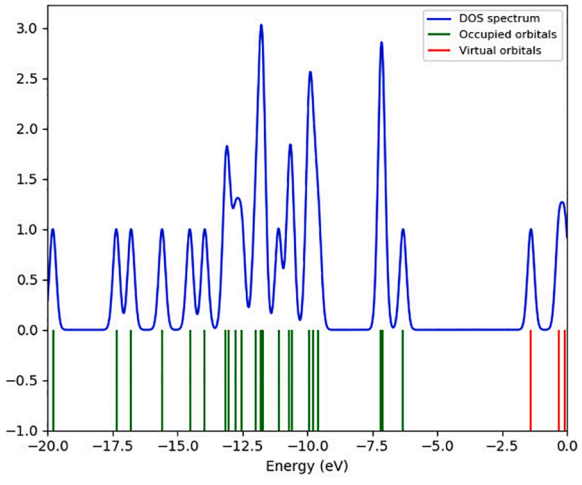

Fig. 9. Density of States (DOS) graph of 1P1 3B.

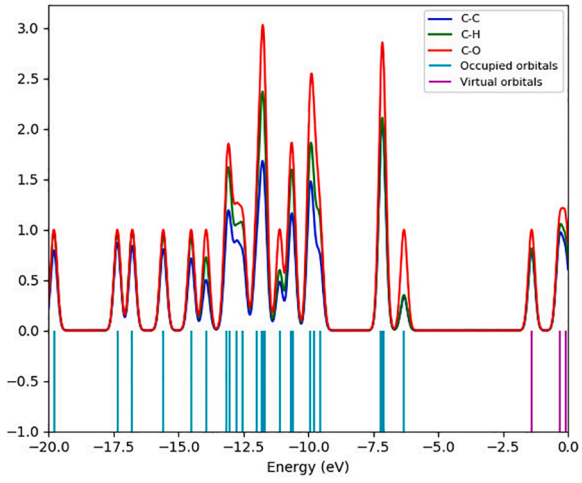

Fig. 10. Projected Density of States (PDOS) graph of 1P1 3B.

Table 6
Calculated drug-like properties for 1P1 3B molecule.

Descriptor	value
Hydrogen Bond Donor (HBD)	0
Hydrogen Bond Acceptor (HBA)	2
AlogP	0.725
Topological polar surface area (TPSA)	34.14
Number of atoms	22
Number of rotatable bonds	1
Molecular weight	162.19

4.10. Molecular docking

In recent years, numerous researchers have determined the biological property to be the most important parameter for organic molecules. In this context, protein receptors appropriate for in silico analysis have been selected from a protein data bank. The ligand (header chemical) to a certain protein receptor binding site is predicted, and the highest rank

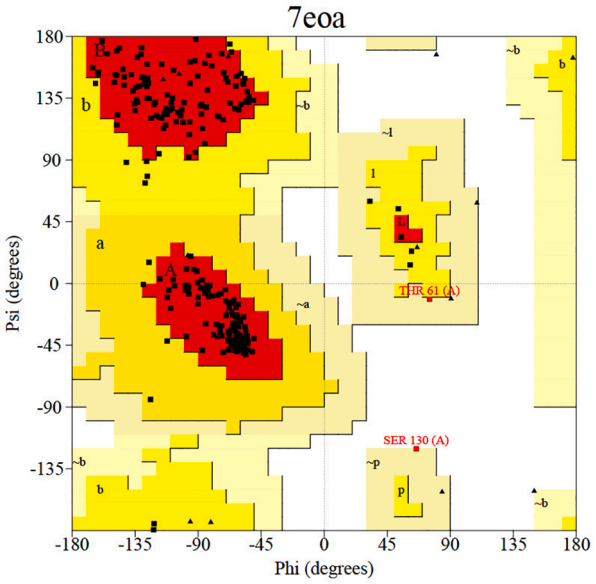

Fig. 11. Ramachandran plot for protein 7EOA.

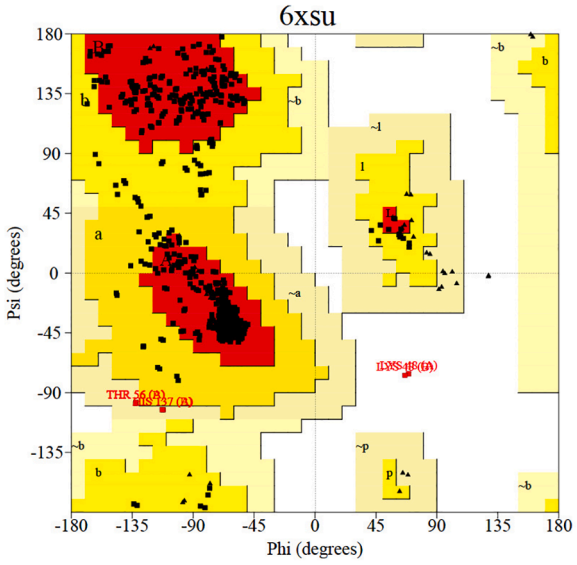

Fig. 12. Ramachandran plot for protein 6XSU.

cluster configuration scoring molecules with the best binding energy function are identified. To learn more about the docking process at the molecular level and to design complex 3D structures, Auto-Dock 4.2.6 is utilized. A survey of the relevant published research reveals that benzoylacetone compounds exhibit powerful hydrolase and antibody behaviour. PASS Online is the software used to predict the pharmaceutical activity of a compound. The investigated chemical is paired with the hydrolase proteins 7EOA, 6XSU, and antibody protein 5K59 in the docking process [77–79]. The molecular docking binding energies for 7EOA, 6XSU, and 5K59 are -3.85, -4.60 and - 4.30 kcal/mol, respectively, in spite of the fact that the inhibition constants are 361.51, 424.68 and 410.03μm, and the inter- molecular energy is -4.74, -5.50 and -5.19 kcal/mol. Table 7 shows the characteristics of the molecule's docking position in regard to the protein 6XSU that is being targeted and had the proteins with the least amount of binding energy, with a value of -4.60 kcal/mol, and the vast majority of the inhibitors had some kind of interaction with the ligand at the 6XSU bonding point. They had three hydrogen bonds, and their inhibition constant of 424.68μm and an

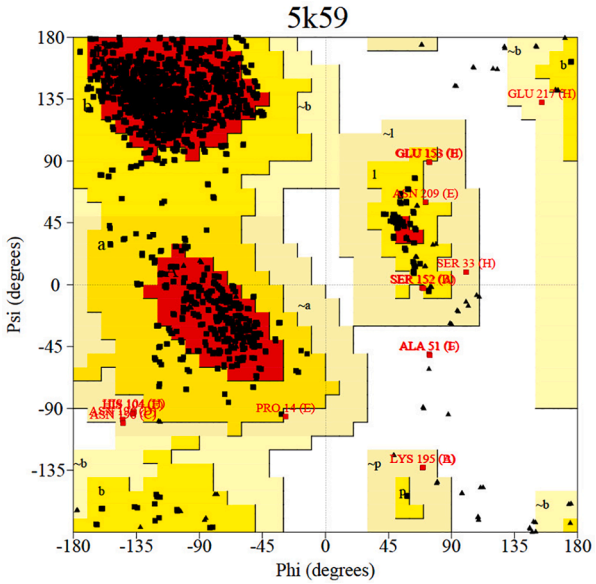

Fig. 13. Ramachandran plot for protein 5K59.

RMSD of 84.24 involving ANS74, TRP180 and GLU297. Figs. 14-16 show how the ligand interacts with three different receptors.

5. Conclusion

The experimental and theoretical FTIR and FT Raman spectra were compared, and notable peaks were analysed in more detail. There were 60 different vibrational modes in the molecule under study, and all of them have been assigned. The HOMO and LUMO energy levels of 1P1 3B were determined using frontiers. Absorption peaks were seen in the UV-Vis spectra at 335.90 nm, 281.18 nm, 232.11 nm, and 249.11 nm (for gas), and at 364 nm, 317 nm, 270 nm, and 219 nm (for DMSO). The energy gap and global reactivity parameters were computed using this data and this reflects the molecular stability. The biological activity of 1P1 3B was established by calculating the electrophilicity index. The computed chemical softness value explains the low toxicity of 1P1 3B. All active sites were investigated using 2D color-coded MEP and ELF maps. NBO was utilised to identify intermolecular and intramolecular interactions. Stability of the molecule was figured out by computing the lone pair transitions, σ to σ * transitions, and π to π * transitions. Donors interacting with nearby anti-bonding acceptors are analysed in terms of their LP(O5) and LP(O6) stabilization energies. The compound satisfies Lipinski's rule, Veber's rule, and the Ghose filter. In addition, molecular docking simulations have been carried out using protein targets 7EOA, 6XSU, and 5K59 that have been shown to demonstrate the biological activity. The three targeted proteins had minimum binding energies of −3.85 kcal/mol, −4.60 kcal/mol, and −4.30 kcal/mol, respectively.

CRediT authorship contribution statement

M. Lawrence: Conceptualization, Data curation, Formal analysis, Visualization. **E. Isac Paulraj:** Data curation, Writing – original draft, Visualization, Investigation, Writing – review & editing. **P. Rajesh:** Supervision, Validation, Software, Visualization, Methodology.

Declaration of Competing Interest

The authors declare that they have no known competing financial interests or personal relationships that could have appeared to influence the work reported in this paper.

Table 7
Molecular docking of 1P1 3B molecule with antagonist protein target.

Protein ID	Residues	Bond Length (Å)	Inhibition constant (μm)	Binding energy (kcal/mol)	Intermolecular energy (kcal/mol)	RMSD (Å)
7EOA	THR169	2.0	361.51	-3.85	-4.74	89.40
	LEU210	2.2				
	GLU294	2.9				
6XSU	ANS74	2.0	424.68	-4.60	-5.50	84.24
	TRP180	2.2				
	GLU297	2.9				
5K59	THR52	3.0	410.03	-4.30	-5.19	88.65
	HIS237	3.1				
	THR97	3.1				
	THR100	3.2				

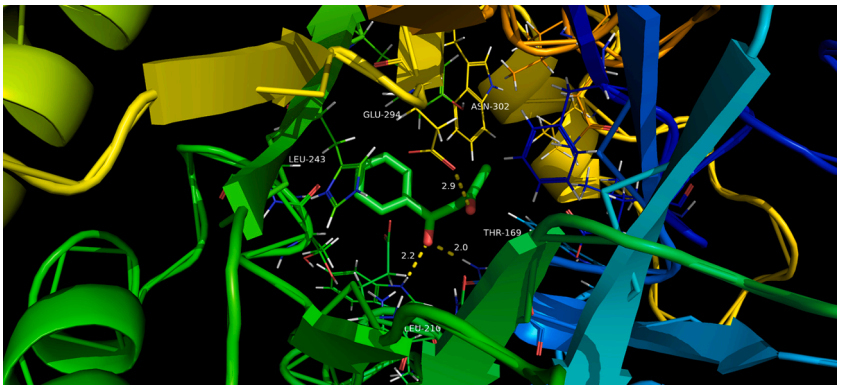

Fig. 14. Docking the hydrogen bond interactions of 1P1 3B with 7EOA protein.

Fig. 15. Docking the hydrogen bond interactions of 1P1 3B with 6XSU protein.

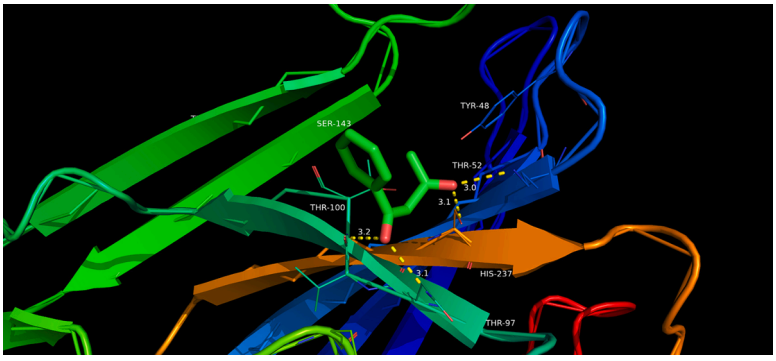

Fig. 16. Docking the hydrogen bond interactions of 1P1 3B with 5K59 protein.

Data availability

Data will be made available on request.

Supplementary materials

Supplementary material associated with this article can be found, in the online version, at doi:10.1016/j.chphi.2023.100226.

References

[1] Y. Morimoto, F. Matsuda, H. Shirahama, Total synthesis of (±)-virantmycin and determination of its stereochemistry, Synlett 03 (1991) 202–203, https://doi.org/10.1055/s-1991-20680.

[2] J.P. Michael, Quinoline, quinazoline and acridone alkaloids, Nat. Prod. Rep. 16 (6) (1999) 697–709, https://doi.org/10.1039/a809408j.

[3] D.G. Markees, V.C. Dewey, G.W. Kidder, Antiprotozoal 4-aryloxy-2-aminoquinolines and related compounds, J. Med. Chem. 13 (2) (1970) 324–326, https://doi.org/10.1021/jm00296a048.

[4] S.F. Campbell, J.D. Hardstone, M.J. Palmer, 2,4-Diamino-6,7-dimethoxyquinoline derivatives as .alpha.1-adrenoceptor antagonists and antihypertensive agents, J. Med. Chem. 31 (5) (1988) 1031–1035, https://doi.org/10.1021/jm00400a025.

[5] M.L. Eidinoff, Dissociation constants of acetylacetone, ethyl acetoacetate and benzoylacetone, J. Am. Chem. Soc. 67 (12) (1945) 2072–2073, https://doi.org/10.1021/ja01228a005.

[6] A. Ramalingam, S. Kansız, N. Dege, S. Sambandam, Synthesis, crystal structure, DFT calculations and hirshfeld surface analysis of 3-Chloro-2,6-Bis(4-Chlorophenyl)-3-methylpiperidin-4-one, J. Chem. Crystallogr. 51 (2) (2020) 273–287, https://doi.org/10.1007/s10870-020-00852-3.

[7] S. Kansız, A.M. Qadir, N. Dege, S.H. Faizi, Two new copper (II) carboxylate complexes based on N, N, N', N'-tetramethylethyleneamine: Synthesis, crystal structures, spectral properties, dft studies and hirshfeld surface analysis, J. Mol. Struct. 1230 (2021), 129916, https://doi.org/10.1016/j.molstruc.2021.129916.

[8] I. Sayer, N. Dege, H. Ghalla, A. Moliterni, H. Naïli, Crystal structure, DFT studies and thermal characterization of new luminescent stannate (IV) based inorganic-organic hybrid compound, J. Mol. Struct. 1224 (2021), 129266, https://doi.org/10.1016/j.molstruc.2020.129266.

[9] G. Demirtaş, N. Dege, H. İçbudak, Ö. Yurdakul, O. Büyükgüngör, Experimental and DFT Studies on Poly[di-μ3-acesulfamato-O, O:O′;O′:O,O-di-μ-acesulfamato-O,O; N-di-μ-aqua-dicalcium(II)], Complex. J. Inorg. Organomet. 22 (4) (2012) 671–679, https://doi.org/10.1007/s10904-012-9679-7.

[10] S. Demir, S. Cakmak, N. Dege, H. Kutuk, M. Odabasoglu, R.A. Kepekci, A novel 3-acetoxy-2-methyl-N-(4-methoxyphenyl)benzamide: Molecular structural describe, antioxidant activity with use X-ray diffractions and DFT calculations, J. Mol. Struct. 1100 (2015) 582–591, https://doi.org/10.1016/j.molstruc.2015.08.014.

[11] S. Kansız, A. Tolan, M. Azam, N. Dege, M. Alam, Y. Sert, S.I. Al-Resayes, H. İçbudak, Acesulfame based Co(II) complex: synthesis, structural investigations, solvatochromism, Hirshfeld surface analysis and molecular docking studies, Polyhedron 218 (2022), 115762, https://doi.org/10.1016/j.poly.2022.115762.

[12] R. Ilmi, D. Zhang, J.D.L. Dutra, N. Dege, L. Zhou, W.Y. Wong, P.R. Raithby, M. S. Khan, A tris β-diketonate europium(III) complex based OLED fabricated by thermal evaporation method displaying efficient bright red emission, Org. Electron. 96 (2021), 106216, https://doi.org/10.1016/j.orgel.2021.106216.

[13] M. Muslim, A. Ali, I. Neogi, N. Dege, M. Shahid, M. Ahmad, Facile synthesis, topological study, and adsorption properties of a novel Co (II)-based coordination polymer for adsorptive removal of methylene blue and methyl orange dyes, Polyhedron 210 (2021), 115519, https://doi.org/10.1016/j.poly.2021.115519.

[14] S. Gatfaoui, N. Issaoui, A. Mezni, F. Bardak, T. Roisnel, A. Atac, H. Marouani, Synthesis, structural and spectroscopic features, and investigation of bioactive nature of a novel organic-inorganic hybrid material 1H-1,2,4-triazole-4-ium trioxonitrate, J. Mol. Struct. 1150 (2017) 242–257, https://doi.org/10.1016/j.molstruc.2017.08.092.

[15] Ö. Tamer, N. Dege, G. Demirtaş, D. Avcı, Y. Atalay, M. Macit, A.A. Ağar, An experimental and theoretical study on the novel (Z)-1-((naphthalen-2-ylamino) methylene)naphthalen-2(1H)-one crystal, Spectrochim. Acta Part A 117 (2014) 13–23, https://doi.org/10.1016/j.saa.2013.07.098.

[16] F.E. Kalai, K. Karrouchi, C. Baydere, S. Daoui, M. Allali, N. Dege, N. Benchat, S. A. Brandán, Synthesis, crystal structure, spectroscopic studies, NBO, AIM and SQMFF calculations of new pyridazinone derivative, J. Mol. Struct. 1223 (2021), 129213, https://doi.org/10.1016/j.molstruc.2020.129213.

[17] M. Ashfaq, K.S. Munawar, M.N. Tahir, N. Dege, M. Yaman, S. Muhammad, S. S. Alarfaji, H. Kargar, M.U. Arshad, Synthesis, crystal structure, Hirshfeld surface analysis, and computational study of a novel organic salt obtained from benzylamine and an acidic component, ACS Omega 6 (34) (2021) 22357–22366, https://doi.org/10.1021/acsomega.1c03078.

[18] N. Dege, H. Içbudak, E. Adıyaman, Bis(acesulfamato-κ2O4,N)bis(3-methylpyridine)copper(II), Acta Crystallogr. Sect. C Cryst. Struct. Commun. 62 (9) (2006) m401–m403, https://doi.org/10.1107/s0108270106027880.

[19] E. Aydemir, S. Kansiz, M.K. Gumus, N.Yu. Gorobets, N. Dege, Crystal structure and Hirshfeld surface analysis of 7-ethoxy-5-methyl-2-(pyridin-3-yl)-11,12-dihydro-5,11-methano[1,2,4]triazolo[1,5-c][1,3,5]benzoxadiazocine, Acta Crystallogr. Sect. C Struct. Rep. Online 74 (3) (2018) 367–370, https://doi.org/10.1107/s2056989018002621.

[20] N. Issaoui, H. Ghalla, F. Bardak, M. Karabacak, N. AouledDlala, H. Flakus, B. Oujia, Combined experimental and theoretical studies on the molecular structures, spectroscopy, and inhibitor activity of 3-(2-thienyl)acrylic acid through AIM, NBO, FT-IR, FT-Raman, UV and HOMO-LUMO analyses, and molecular docking, J. Mol. Struct. 1130 (2017) 659–668, https://doi.org/10.1016/j.molstruc.2016.11.019.

[21] A.S. Kazachenko, F. Akman, A. Sagaama, N. Issaoui, Y.N. Malyar, N.Y. Vasilieva, V. S. Borovkova, Theoretical and experimental study of guar gum sulfation, J. Mol. Model. 27 (1) (2021), https://doi.org/10.1007/s00894-020-04645-5.

[22] A. Ramalingam, S. Sambandam, M. Medimagh, O. Al-Dossary, N. Issaoui, M. Wojcik, Study of a new piperidone as an anti-Alzheimer agent: Molecular docking, electronic and intermolecular interaction investigations by DFT method, J. Univ. Sci. 33 (8) (2021), 101632, https://doi.org/10.1016/j.jksus.2021.101632.

[23] P. Sen, G.Y. Atmaca, A. Erdogmus, S.D. Kanmazalp, N. Dege, S.Z. Yildiz, Peripherally tetra-benzimidazole units-substituted zinc(II) phthalocyanines: Synthesis, characterization and investigation of photophysical and photochemical properties, J. Lumin. 194 (2018) 123–130, https://doi.org/10.1016/j.jlumin.2017.10.022.

[24] M. Kurbanova, M. Ashfaq, M.N. Tahir, A. Maharramov, N. Dege, N. Ramazanzade, M. Kurbanova, M. Ashfaq, M.N. Tahir, A. Maharramov, N. Dege, A. Koroglu, Synthesis, crystal structure, supramolecular assembly exploration by hirshfeld surface analysis and computational study of 6-bromo-2-oxo- 2h-chromene-3-carbonitrile (BOCC), J. Struct. Chem. 64 (2) (2023) 302–313, https://doi.org/10.1134/s0022476623020142.

[25] S. Kansiz, N. Dege, S. Ozturk, N. Akdemir, E. Tarcan, A. Arslanhan, E. Saif, Crystal structure and Hirshfeld surface analysis of 2-methyl-3-nitro-N-[(E)-(5-nitrothiophen-2-yl)methylidene]aniline, Acta Crystallogr. Sect. C Struct. Rep. Online 77 (2) (2021) 138–141, https://doi.org/10.1107/s2056989021000529.

[26] S. Hamamci Alisir, N. Dege, A new antibacterial silver(I) complex incorporating 2,5-dimethylpyrazine and the anti-inflammatory diclofenac, Acta Crystallogr. Sect. Cryst. Struct. Commun. 72 (12) (2016) 947–951, https://doi.org/10.1107/s2053229616017009.

[27] S. Hamamci Alisir, N. Dege, R. Tapramaz, Synthesis, crystal structures and characterizations of three new copper(II) complexes including anti-inflammatory diclofenac, Acta Crystallogr. Sect. C Cryst. Struct. Commun. 75 (4) (2019) 388–397, https://doi.org/10.1107/s2053229619001827.

[28] Gaussian09, R. A. 1, frisch , trucks , schlegel , scuseria , robb , cheeseman , Scalmani g., Barone v., Mennucci b., petersson et al., gaussian. Inc., Wallingford CT. 121 (2009) 150-166.

[29] M. Evecen, H. Tanak, F. Tinmaz, N. Dege, İ. Özer İlhan, Experimental (XRD, IR and NMR) and theoretical investigations on 1-(2-nitrobenzoyl)3,5-bis(4-methoxyphenyl)-4,5-dihydro-1H-pyrazole, J. Mol. Struct. 1126 (2016) 117–126, https://doi.org/10.1016/j.molstruc.2016.01.069.

[30] Zhurko, G., Zhurko, D. Chemcraft, Version 1.7 (build 365) (2013) http://www.chemcraftprog.com (accessed March 27, 2016).

[31] W. LI, H. Xie, Y. Huang, L. Song, Y. Shao, K. Qiu, Application of Gaussian 09/GaussView 5.0 in analytical chemistry teaching, J. Kunming Med. Univ. (2016) 134–136.

[32] M.H. Jomroz, Vibrational Energy Distribution Analysis, VEDA4, ScienceOpen. Inc., Warsaw, Poland, 2004.

[33] A. Stash, V. Tsirelson, WinXPRO: a program for calculating crystal and molecular properties using multipole parameters of the electron density, J. Appl. Crystallogr. 35 (3) (2002) 371–373, https://doi.org/10.1107/s0021889802003230.

[34] New NIST standard reference database 38, Chemom. Intell. Lab. Syst. 14 (1–3) (1992) 434–435, https://doi.org/10.1016/0169-7439(92)80129-r.

[35] I.M. Alecu, J. Zheng, Y. Zhao, D.G. Truhlar, Computational thermochemistry: scale factor databases and scale factors for vibrational frequencies obtained from electronic model chemistries, J. Chem. Theory Comput. 6 (9) (2010) 2872–2887, https://doi.org/10.1021/ct100326h.

[36] M.E. Casida, Time-dependent density functional response theory of molecular systems: theory, computational methods, and functionals, Recent Dev. Appl. Mod. Density Funct. Theory (1996) 391–439, https://doi.org/10.1016/s1380-7323(96)80093-8.

[37] M.E. Casida, Time-dependent density functional response theory for molecules, Recent Adv. Comput. Chem. (1995) 155–192, https://doi.org/10.1142/9789812830586_0005.

[38] Marques, M. A. L., Maitra, N. T., Nogueira, F. M. S., et al., (Eds.) Fundamentals of Time-Dependent Density Functional Theory. Lecture Notes in Physics (2012) 10.1007/978-3-642-23518-4.

[39] T. Lu, F. Chen, Multiwfn: a multifunctional wavefunction analyzer, J. Comput. Chem. 33 (5) (2011) 580–592, https://doi.org/10.1002/jcc.22885.

[40] N.M. O'boyle, A.L. Tenderholt, K.M. Langner, A library for package-independent computational chemistry algorithms, J. Comput. Chem. 29 (5) (2008) 839–845, https://doi.org/10.1002/jcc.20823.

[41] İ. Koyuncu, M. Durgun, N. Yorulmaz, S. Toprak, A. Gonel, N. Bayraktar, M. Caglayan, Molecular docking demonstration of the liquorice chemical molecules on the protease and ACE2 of COVID-19 virus, Curr. Enzyme Inhib. 17 (2) (2021) 98–110, https://doi.org/10.2174/1573408016999201228193118.

[42] X. Chen, L. Liu, Congenital cataract with LSS gene mutations: a new case report, J. Pediatr. Endocrinol. Metab. 30 (11) (2017), https://doi.org/10.1515/jpem-2017-0101.

[43] K.A. Rostomily, D.M. Jones, C.M. Pautz, D.W. Ito, M.J. Buono, Haemoconcentration, not decreased blood temperature, increases blood viscosity during cold water immersion, Diving Hyperb. Med. 50 (1) (2020) 24–27, https://doi.org/10.28920/dhm50.1.24-27.

[44] R.A. Laskowski, M.B. Swindells, LigPlot+: multiple ligand–protein interaction diagrams for drug discovery, J. Chem. Inf. Model. 51 (10) (2011) 2778–2786, https://doi.org/10.1021/ci200227u.
[45] E.F. Pettersen, T.D. Goddard, C.C. Huang, G.S. Couch, D.M. Greenblatt, E.C. Meng, T.E. Ferrin, UCSF Chimera?A visualization system for exploratory research and analysis, J. Comput. Chem. 25 (13) (2004) 1605–1612, https://doi.org/10.1002/jcc.20084.
[46] S.H. Alisir, N. Ozdemir, E. Burgaz, N. Dege, Y.E. Canavar, Fabrication and antimicrobial activity of poly(lactic acid) nanofibers containing firstly synthesized silver diclofenac complex with (2-methylimidazole) for wound dressing applications, Fibers Polym. 22 (10) (2021) 2738–2749, https://doi.org/10.1007/s12221-021-0166-z.
[47] R. Ilmi, S. Kansız, N. Dege, M.S. Khan, Synthesis, structure, Hirshfeld surface analysis and photophysical studies of red emitting europium acetylacetonate complex incorporating a phenanthroline derivative, J. Photochem. Photobiol. A 377 (2019) 268–281, https://doi.org/10.1016/j.jphotochem.2019.03.036.
[48] W. Guerrab, I.M. Chung, S. Kansiz, J.T. Mague, N. Dege, J. Taoufik, R. Salghi, I. H. Ali, M.I. Khan, H. Lgaz, Y. Ramli, Synthesis, structural and molecular characterization of 2,2-diphenyl-2H,3H,5H,6H,7H-imidazo[2,1-b][1,3]thiazin-3-one, J. Mol. Struct 1197 (2019) 369–376, https://doi.org/10.1016/j.molstruc.2019.07.081.
[49] S. Demir, A.O. Sarioğlu, S. Güler, N. Dege, M. Sönmez, Synthesis, crystal structure analysis, spectral IR, NMR UV–Vis investigations, NBO and NLO of 2-benzoyl-N-(4-chlorophenyl)-3-oxo-3-phenylpropanamide with use of X-ray diffractions studies along with DFT calculations, J. Mol. Struct. 1118 (2016) 316–324, https://doi.org/10.1016/j.molstruc.2016.04.042.
[50] F.H. Herbstein, B.B. Iversen, M. Kapon, F.K. Larsen, G.K.H. Madsen, G.M. Reisner, X-ray and neutron diffraction study of benzoylacetone in the temperature range 8–300 K: comparison with other cis-enol molecules, Acta Crystallogr. Sect. B Struct. Sci. 55 (5) (1999) 767–787, https://doi.org/10.1107/s0108768199004279.
[51] D.A. Long, Infrared and Raman characteristic group frequencies. Tables and chartsGeorge Socrates John Wiley and Sons, Ltd, Chichester, Third Edition, 2001, J. Raman Spectrosc. 35 (10) (2004), https://doi.org/10.1002/jrs.1238, 905–905.
[52] A.G. Severdia, Raman spectroscopic identification of α-zearalanol in intact implants, Appl. Spectrosc. 44 (10) (1990) 1721–1722, https://doi.org/10.1366/0003702904417607.
[53] S. Muthu, E.I. Paulraj, Molecular structure, vibrational spectra, first order hyper polarizability, NBO and HOMO–LUMO analysis of 4-amino-3(4-chlorophenyl) butanoic acid, Solid State Sci. 14 (4) (2012) 476–487, https://doi.org/10.1016/j.solidstatesciences.2012.01.028.
[54] S. Muthu, E. Isac Paulraj, Spectroscopic and molecular structure (monomeric and dimeric structure) investigation of 2-[(2-hydroxyphenyl) carbonyloxy] benzoic acid by DFT method: a combined experimental and theoretical study, J. Mol. Struct. 1038 (2013) 145–162, https://doi.org/10.1016/j.molstruc.2013.01.043.
[55] E. Isac Paulraj, S. Muthu, Spectroscopic studies (FTIR, FT-Raman and UV), potential energy surface scan, normal coordinate analysis and NBO analysis of (2R,3R,4R,5S)-1-(2-hydroxyethyl)-2-(hydroxymethyl) piperidine-3,4,5-triol by DFT methods, Spectrochim. Acta Part A 108 (2013) 38–49, https://doi.org/10.1016/j.saa.2013.01.061.
[56] R. Ramarajan, A. Ramalingam, C. Duraisamy, S. Sambandam, N. ISSAOUI, O.M. Al-Dossary, L.G. Bousiakoug, Catalytic multicomponent synthesis, biological evaluation, molecular docking and in silico ADMET studies of some novel 3-alkyl indoles, J. King Saud Univ. Sci. 35 (2) (2023), 102475, https://doi.org/10.1016/j.jksus.2022.102475.
[57] N. Rekik, N. Issaoui, H. Ghalla, B. Oujia, M.J. Wójcik, IR spectral density of H-bonds. Both intrinsic anharmonicity of the fast mode and the H-bond bridge. Part I: Anharmonic coupling parameter and temperature effects, J. Mol. Struct. Theochem. 821 (1) (2007) 9–21, https://doi.org/10.1016/j.theochem.2007.06.016.
[58] Lin-Vien, D., Colthup, N.B., Fateley, W.G., Grasselli, J.G. Preface. The Handbook of Infrared and Raman Characteristic Frequencies of Organic Molecules. (1991) xv–xvi. 10.1016/b978-0-08-057116-4.50005-5.
[59] C. Puzzarini, M. Biczysko, V. Barone, Accurate anharmonic vibrational frequencies for uracil: the performance of composite schemes and hybrid CC/DFT model, J. Chem. Theory Comput. 7 (11) (2011) 3702–3710, https://doi.org/10.1021/ct200552m.
[60] N. Rekik, N. Issaoui, B. Oujia, M.J. Wójcik, Theoretical IR spectral density of H-bond in liquid phase: combined effects of anharmonicities, Fermi resonances, direct and indirect relaxations, J. Mol. Liq. 141 (3) (2008) 104–109, https://doi.org/10.1016/j.molliq.2007.10.009.
[61] N. Issaoui, N. Rekik, B. Oujia, M.J. Wójcik, Theoretical infrared line shapes of H-bonds within the strong anharmonic coupling theory and Fermi resonances effects, Int. J. Quantum Chem. 110 (14) (2010) 2583–2602, https://doi.org/10.1002/qua.22395.
[62] S. Muthu, E. Isac Paulraj, Molecular structure and spectroscopic characterization of ethyl 4-aminobenzoate with experimental techniques and DFT quantum chemical calculations, Spectrochim. Acta Part A. 112 (2013) 169–181, https://doi.org/10.1016/j.saa.2013.04.024.
[63] E. Isac Paulraj, S. Muthu, Molecular structure analysis and spectroscopic characterization of 5-ethyl-5-phenyl-1,3-diazinane-4,6-dione with experimental (FT-IR and FT-Raman) techniques and quantum chemical calculations, Spectrochim. Acta Part A. 106 (2013) 310–320, https://doi.org/10.1016/j.saa.2013.01.048.
[64] A. Fokkens, P. Vossen, M. Rospocher, R. Hoekstra, W.R. van Hage, GRaSP: grounded representation and source perspective, in: Proceedings of the Workshop Knowledge Resources for the Socio-Economic Sciences and Humanities, 2017, https://doi.org/10.26615/978-954-452-040-3_003.
[65] S. Singh, H. Singh, T. Karthick, P. Tandon, D.H. Dethe, R.D. Erande, Conformational study and vibrational spectroscopic (FT-IR and FT-Raman) analysis of an alkaloid-borreverine derivative, Anal. Sci. 33 (1) (2017) 99–104, https://doi.org/10.2116/analsci.33.99.
[66] M. Govindarajan, M. Karabacak, Spectroscopic properties, NLO, HOMO–LUMO and NBO analysis of 2,5-Lutidine, Spectrochim. Acta Part A 96 (2012) 421–435, https://doi.org/10.1016/j.saa.2012.05.067.
[67] H. Jacobsen, Localized-orbital locator (LOL) profiles of chemical bonding, Can. J. Chem. 86 (7) (2008) 695–702, https://doi.org/10.1139/v08-052.
[68] S. Muthu, G. Ramachandran, E. Isac Paulraj, T. Swaminathan, Quantum mechanical study of the structure and spectroscopic (FTIR, FT-Raman), first-order hyperpolarizability and NBO analysis of 1,2-benzoxazol-3-ylmenthane sulfonamide, Spectrochim. Acta Part A 128 (2014) 603–613, https://doi.org/10.1016/j.saa.2014.02.183.
[69] C.B. Aakeröy, M. Nieuwenhuyzen, S.L. Price, Three polymorphs of 2-amino-5-nitropyrimidine: experimental structures and theoretical predictions, J. Am. Chem. Soc. 120 (35) (1998) 8986–8993, https://doi.org/10.1021/ja981122i.
[70] V. Tsirelson, A. Stash, Determination of the electron localization function from electron density, Chem. Phys. Lett. 351 (1–2) (2002) 142–148, https://doi.org/10.1016/s0009-2614(01)01361-6.
[71] V. Vijayakumar, A. Prabakaran, N. Radhakrishnan, S. Muthu, C. Rameshkumar, E. Isac Paulraj, Synthesis, characterization, spectroscopic studies, DFT and molecular docking analysis of N, N′-dibutyl-3, 3′-diaminobenzidine, J. Mol. Struct. 1179 (2019) 325–335, https://doi.org/10.1016/j.molstruc.2018.11.018.
[72] S. Muthu, M. Prasath, E. Isac Paulraj, R. Arun Balaji, FT-IR, FT-Raman spectra and ab initio HF and DFT calculations of 7-chloro-5-(2-chlorophenyl)-3-hydroxy-2,3-dihydro-1H-1,4-benzodiazepin-2-one, Spectrochim. Acta Part A 120 (2014) 185–194, https://doi.org/10.1016/j.saa.2013.09.150.
[73] C.A. Lipinski, F. Lombardo, B.W. Dominy, P.J. Feeney, Experimental and computational approaches to estimate solubility and permeability in drug discovery and development settings, Adv. Drug Deliv. Rev. 23 (1–3) (1997) 3–25, https://doi.org/10.1016/s0169-409x(96)00423-1.
[74] C.A. Lipinski, Lead- and drug-like compounds: the rule-of-five revolution, Drug Discov. Today 1 (4) (2004) 337–341, https://doi.org/10.1016/j.ddtec.2004.11.007.
[75] R.S. Saji, J.C. Prasana, S. Muthu, J. George, T.K. Kuruvilla, B.R. Raajaraman, Spectroscopic and quantum computational study on naproxen sodium, Spectrochim. Acta Part A 226 (2020), 117614, https://doi.org/10.1016/j.saa.2019.117614.
[76] W.P. Walters, M.A. Murcko, Prediction of 'drug-likeness, Adv. Drug Deliv. Rev. 54 (3) (2002) 255–271, https://doi.org/10.1016/s0169-409x(02)00003-0.
[77] N. Dege, H. Gökce, O.E. Doğan, G. Alpaslan, T. Ağar, S. Muthu, Y. Sert, Quantum computational, spectroscopic investigations on N-(2-((2-chloro-4,5-dicyanophenyl) amino)ethyl)-4-methylbenzenesulfonamide by DFT/TD-DFT with different solvents, molecular docking and drug-likeness researches, Colloids Surf. A 638 (2022), 128311, https://doi.org/10.1016/j.colsurfa.2022.128311.
[78] F.Z. Boudjenane, F. Triki-Baara, N. Boukabcha, N.E.H. Belkafouf, N. Dege, M. Saidj, N. Khelloul, A. Djafri, A. Chouaih, Synthesis, crystallographic and spectroscopic investigation, chemical reactivity, hyperpolarizabilities and in silico molecular docking study of (Z)-2N-(tert-butylimino)-3N'-(4-methoxyphenyl) thiazolidin-4-one, J. Mol. Struct. (2023), 135620, https://doi.org/10.1016/j.molstruc.2023.135620.
[79] Ö. Tamer, H. Mahmoody, K.F. Feyzioğlu, O. Kılınç, D. Avci, O. Orun, N. Dege, Y. Atalay, Synthesis of the first mixed ligand Mn (II) and Cd (II) complexes of 4-methoxy-pyridine-2-carboxylic acid, molecular docking studies and investigation of their anti-tumor effectsin vitro, Appl. Organomet. Chem. 34 (3) (2019), https://doi.org/10.1002/aoc.5416. Portico.